High-Risk Mucosal Human Papillomavirus 16 (HPV16) E6 Protein and Cutaneous HPV5 and HPV8 E6 Proteins Employ Distinct Strategies To Interfere with Interferon Regulatory Factor 3-Mediated Beta Interferon Expression

Juline Poirson, Irina Paula Suarez, Marie-Laure Straub, Alexandra Cousido-Siah, Paul Peixoto, Eric Hervouet, Anne Foster, André Mitschler, Noella Mukobo, Yassmine Chebaro, et al.

AMERICAN SOCIETY FOR MICROBIOLOGY | Journal of Virology®

VIRUS-CELL INTERACTIONS

High-Risk Mucosal Human Papillomavirus 16 (HPV16) E6 Protein and Cutaneous HPV5 and HPV8 E6 Proteins Employ Distinct Strategies To Interfere with Interferon Regulatory Factor 3-Mediated Beta Interferon Expression

Juline Poirson,[a] Irina Paula Suarez,[b] Marie-Laure Straub,[a] Alexandra Cousido-Siah,[b] Paul Peixoto,[c] Eric Hervouet,[c] Anne Foster,[a] André Mitschler,[b] Noella Mukobo,[a] Yassmine Chebaro,[b] Dominique Garcin,[d] Sevda Recberlik,[e] Christian Gaiddon,[e] Danièle Altschuh,[b] Yves Nominé,[b] Alberto Podjarny,[b] Gilles Trave,[b] Murielle Masson[a]

[a]Equipe Signalisation Nucléaire, UMR 7242, CNRS, Université de Strasbourg, Ecole Supérieure de Biotechnologie de Strasbourg (ESBS), Illkirch, France
[b]Equipe Labellisée Ligue 2015, Department of Integrated Structural Biology, Institut de Génétique et de Biologie Moléculaire et Cellulaire (IGBMC), INSERM U1258, CNRS UMR 7104, Université de Strasbourg, Illkirch, France
[c]Equipe TIM-C, groupe "Autophagy, EMT and antitumor T-cell immunity," INSERM UMR1098, Laboratoire de Biochimie, Besançon, France
[d]Department of Microbiology and Molecular Medicine, University of Geneva School of Medicine, Geneva, Switzerland
[e]Equipe Streinth, INSERM U1113, Strasbourg, France

ABSTRACT Persistent infection with some mucosal α-genus human papillomaviruses (HPVs; the most prevalent one being HPV16) can induce cervical carcinoma, anogenital cancers, and a subset of head and neck squamous cell carcinoma (HNSCC). Cutaneous β-genus HPVs (such as HPV5 and HPV8) associate with skin lesions that can progress into squamous cell carcinoma with sun exposure in *Epidermodysplasia verruciformis* patients and immunosuppressed patients. Here, we analyzed mechanisms used by E6 proteins from the α- and β-genus to inhibit the interferon-β (IFNB1) response. HPV16 E6 mediates this effect by a strong direct interaction with interferon regulatory factor 3 (IRF3). The binding site of E6 was localized within a flexible linker between the DNA-binding domain and the IRF-activation domain of IRF3 containing an LxxLL motif. The crystallographic structure of the complex between HPV16 E6 and the LxxLL motif of IRF3 was solved and compared with the structure of HPV16 E6 interacting with the LxxLL motif of the ubiquitin ligase E6AP. In contrast, cutaneous HPV5 and HPV8 E6 proteins bind to the IRF3-binding domain (IBiD) of the CREB-binding protein (CBP), a key transcriptional coactivator in IRF3-mediated IFN-β expression.

IMPORTANCE Persistent HPV infections can be associated with the development of several cancers. The ability to persist depends on the ability of the virus to escape the host immune system. The type I interferon (IFN) system is the first-line antiviral defense strategy. HPVs carry early proteins that can block the activation of IFN-I. Among mucosal α-genus HPV types, the HPV16 E6 protein has a remarkable property to strongly interact with the transcription factor IRF3. Instead, cutaneous HPV5 and HPV8 E6 proteins bind to the IRF3 cofactor CBP. These results highlight the versatility of E6 proteins to interact with different cellular targets. The interaction between the HPV16 E6 protein and IRF3 might contribute to the higher prevalence of HPV16 than that of other high-risk mucosal HPV types in HPV-associated cancers.

KEYWORDS HPV, IRF3, interactomic, interferons, three-dimensional structure

Human papillomaviruses (HPVs) include more than 400 types and infect keratinocytes from the skin (cutaneous type) or from the genital or oral mucosa (mucosal type). They have been classified in genera (α, β, μ, γ, and η genus) according to the sequence of the L1 capsid protein. Some mucosal HPVs (such as HPV6 and HPV11)

Editor Lawrence Banks, International Centre for Genetic Engineering and Biotechnology

Address correspondence to Murielle Masson, murielle.masson@unistra.fr.
The authors declare no conflict of interest.

Received 29 October 2021
Accepted 30 March 2022

have been associated with benign lesions (such as genital warts), whereas a persistent infection with some "high-risk" mucosal HPVs (about 14 HPV types, namely, HPV16, 18, 31, 33, 35, 39, 45, 51, 52, 56, 58, 59, 66, and 68) can induce precancerous lesions that can progress into carcinoma, such as cervical, anogenital, and a subset of head and neck squamous cell carcinoma (HNSCC). HPV16 accounts for 50% of cervical cancers and 90% of HPV+ oropharyngeal cancers (1). Some cutaneous β-type HPVs may act as cocarcinogens with UV radiation in squamous cell carcinoma (SCC). This association was first reported in *Epidermodysplasia verruciformis* (EV) patients, an extremely rare genetic disease that increases the risk of developing HPV-induced SCC (2). HPV5 and HPV8 have been found in 90% of SCC in *Epidermodysplasia verruciformis* patients (3). As a result of immunosuppression, organ transplant recipients also have greater susceptibility to β-HPV infection of the skin and an increased risk of developing SCC (4).

The oncogenic property of HPVs is due to the expression of two viral proteins, namely, E6 and E7 (5). The best characterized function of HPV E7 proteins is binding to the retinoblastoma protein (pRB1) and to induce its degradation. The E6 proteins from the α-genus were shown to bind to the E6AP ubiquitin ligase. Structural studies reveal that the HPV16 E6 protein contains a hydrophobic pocket, which binds a short linear LxxLL motif in E6AP (6). Binding to the E6AP LxxLL peptide stabilizes a large surface on the E6 protein for the binding to the p53 core domain (7). The resulting ternary complex E6/E6AP/p53 induces the p53 polyubiquitination and its proteasomal degradation.

The innate immune system is the first line of host defense against a variety of pathogens. The initiation of innate immune responses relies on the recognition of pathogen-associated molecular patterns (PAMPs) by pattern-recognition receptors (PRRs), including the Toll-like receptors (TLRs), the retinoic acid-inducible gene I-like receptors (RLRs; such as RIG-1 and MDA5), the nucleotide oligomerization domain-like receptors (NLRs), and cytosolic DNA sensors (cGAS/STING and IFI16) (8). Upon recognition of PAMPS, PRRs activate the kinase tank binding kinase 1 (TBK1) and recruit the IRF3 transcription factor leading to IRF3 phosphorylation (9). Phosphorylated IRF3 undergoes dimerization and translocation into the nucleus (10, 11), where it interacts with the transcription factors IRF7, ATF-2/c-Jun, and NF-κB and the transcriptional coactivator CREB binding protein (CBP) to activate the transcription of type I interferon (IFN-α and IFN-β) genes (12, 13). Secreted type I IFNs bind to the IFN-α/β receptor (IFNAR) and signal through the JAK-STAT pathway leading to the expression of hundreds of IFN-stimulated genes (ISGs) (14).

The HPV early proteins (mainly E2, E6, and E7) play major roles in immune evasion. HPV16 and HPV18 E2 proteins were shown to downregulate the expression of the STING protein (15). High-risk HPV E7 proteins can suppress the transcription of the Toll-like receptor 9 gene (16). HPV18 E7 binds directly to the STING protein through its LXCXE motif (17), whereas the HPV16 E7 protein does not interact with STING but instead increases the autophagy-dependent degradation of STING (18). High-risk HPV E7 can also upregulate the expression of the histone methyltransferase SUV9H1, thereby favoring repressive chromatin marks (H3K9me2 and H3K9me3) at the promoter regions of cGAS, STING, and RIG-1 genes (19). By forming a ternary complex with TRIM25 and USP15, HPV16 E6 suppresses the K63-linked ubiquitination of the viral sensor RIG-1 (20). HPV16 E6 can interact with the transcription factor IRF3 (21), whereas the binding of the HPV18 E6 protein to the Tyk2 kinase can explain at least in part the inhibition of the IFN-α-induced JAK-STAT pathway (22).

In this study, we demonstrate that HPV16, HPV5, and HPV8 E6 proteins are able to inhibit the IRF3 pathway and the activation of IFN-β gene transcription. We identified two distinct molecular mechanisms that can account for this activity. On the one hand, the HPV16 E6 protein interacts directly with IRF3 via an LxxLL motif. The crystal structure of the HPV16 E6/IRF3 LxxLL peptide was solved and revealed that the IRF3 peptide binds into the hydrophobic pocket of E6. By using a combination of site-directed mutagenesis, binding, and activity assays, we decipher the requirement for an E6/IRF3-LxxLL peptide interaction by comparison with an E6/E6AP-LxxLL interaction. On the other hand, cutaneous HPV type β1 (HPV5 and HPV8) E6 proteins do not bind IRF3 but rather

to the IRF3-binding domain of CBP, thereby inhibiting the IRF3-mediated IFN-β expression in an alternative manner.

RESULTS

Inhibition of IRF3/IFN-β pathway by HPV E6 proteins. We have investigated the impact of HPV E6 proteins from different HPV types on the innate antiviral defense and more precisely on the IRF3/IFN-β pathway. For this purpose, we used HEK293T cells infected with Sendai virus (SeV) to induce a strong IRF3-dependent IFN-β gene expression (23). HEK293T cells were transfected with pFlag-RIG-1 and pXJ-Flag hemagglutinin (HA) E6 plasmids encoding E6 proteins from diverse HPV types, as follows: high-risk mucosal α-genus (α7, HPV18; α9, HPV16, HPV52, and HPV58) and cutaneous β-genus (β1, HPV5 and HPV8) HPV. Twenty-four hours after transfection, cells were infected with Sendai virus for 6 hours. Total proteins and total mRNAs were extracted. The expression of HPV E6 proteins was verified by Western blotting using anti-HA antibodies (Fig. 1A). We noticed an additional band for HPV18 E6 corresponding very likely to a spliced form (HPV18 E6 *I) (24). The mRNA level of IFN-β (IFNB1) was quantified by reverse transcriptase quantitative PCR (RT-qPCR) (Fig. 1B). We found a stronger reduction of IFN-β mRNA expression in cells expressing E6 from HPV16, HPV5, and HPV8, in contrast to cells expressing HPV18, HPV52, and HPV58 E6. The inhibition of IFN-β gene expression by HPV16, HPV5, and HPV8 E6 proteins was confirmed by using luciferase reporter plasmids, IFN-β-luciferase containing PRD I to IV regions of IFN-β luciferase (Fig. 1C) and IRF3-luciferase, containing IRF3-binding sites (Fig. 1D) containing, the PRD I to IV regions of IFN-β gene promoter (Fig. 1C) and IRF3-binding sites (Fig. 1D). In order to test the inhibition of IFNB1 mRNA induction by HPV16E6 in a more physiological context than HEK293T cells, we followed IFNB1 mRNA induction upon SeV infection. Indeed, the level of IFNB1 mRNA was reduced in keratinocytes expressing the HPV16 E6 protein (LXSN-HPV16) compared to control keratinocytes (LXSN) (Fig. 1E). On the other hand, in SiHa cells, a cervical cancer cell line containing an integrated HPV16 genome, the silencing of E6 expression by small interfering RNA (siRNA) increased the IFNB1 mRNA induction upon SeV infection (Fig. 1F). In addition, the impact of E6 proteins on the transcriptional activity of IRF3 was addressed by using a Gal4(DBD)-IRF3 (ΔDBD) construct (containing the DNA-binding domain [DBD] of Gal4 fused to IRF3, residues 113 to 427, lacking its N-terminal DBD) and a reporter plasmid containing Gal4 binding sequences upstream of the firefly luciferase gene (Fig. 1G). The overexpression of HPV16, HPV5, or HPV8 E6 inhibits the transcriptional activity of Gal4(DBD)-IRF3(ΔDBD), in contrast to HPV18, HPV52, and HPV58 E6 proteins.

Binding of the HPV16 E6 protein to IRF3. The HPV E6 proteins have been shown to interact with some LxxLL motifs present in host cell proteins (25). The best-characterized example is the binding to the LxxLL motif of the cellular ubiquitin ligase E6AP (6). In addition, HPV16 E6 has also been shown to bind directly to IRF3 (21), possibly via a LxxLL peptide motif (26). We tested the interactions of E6 proteins from mucosal α7 (HPV18) and α9 (HPV16, HPV52, HPV58, and HPV33) and cutaneous β1 (HPV5 and HPV8) HPV types with the two LxxLL-containing targets IRF3 and E6AP by using the split *Gaussia princeps* luciferase protein complementation assay, here named GPCA (27, 28). In this assay, E6 proteins were expressed in fusion with the G2 inactive fragment of *Gaussia princeps* luciferase, whereas E6AP or IRF3 were expressed in fusion with the G1 inactive fragment. The expression of the G2-E6 proteins was verified by Western blotting using polyclonal anti-Gaussia luciferase (Gluc) antibodies (Fig. 2A). For HPV18 E6, we observed the expression of a full-length HPV18 E6 protein and the spliced form mentioned before, namely, E6*I. For each protein pair tested in the GPCA assay, we determined a normalized ratio of luminescence (NLR) as defined previously (27). We found that the E6 proteins from the α-genus (HPV16, HPV18, HPV52, HPV58, and HPV33) interacted with E6AP, in contrast to E6 proteins from the β1-genus (HPV5 and HPV8) (Fig. 2B and C). A GPCA signal was obtained with IRF3 and E6 proteins from the α7 group (HPV52, HPV58, and HPV33) but no signal at all with E6 from HPV18, HPV5, and HPV8 types. The highest GPCA signal was obtained with HPV16 E6 and IRF3,

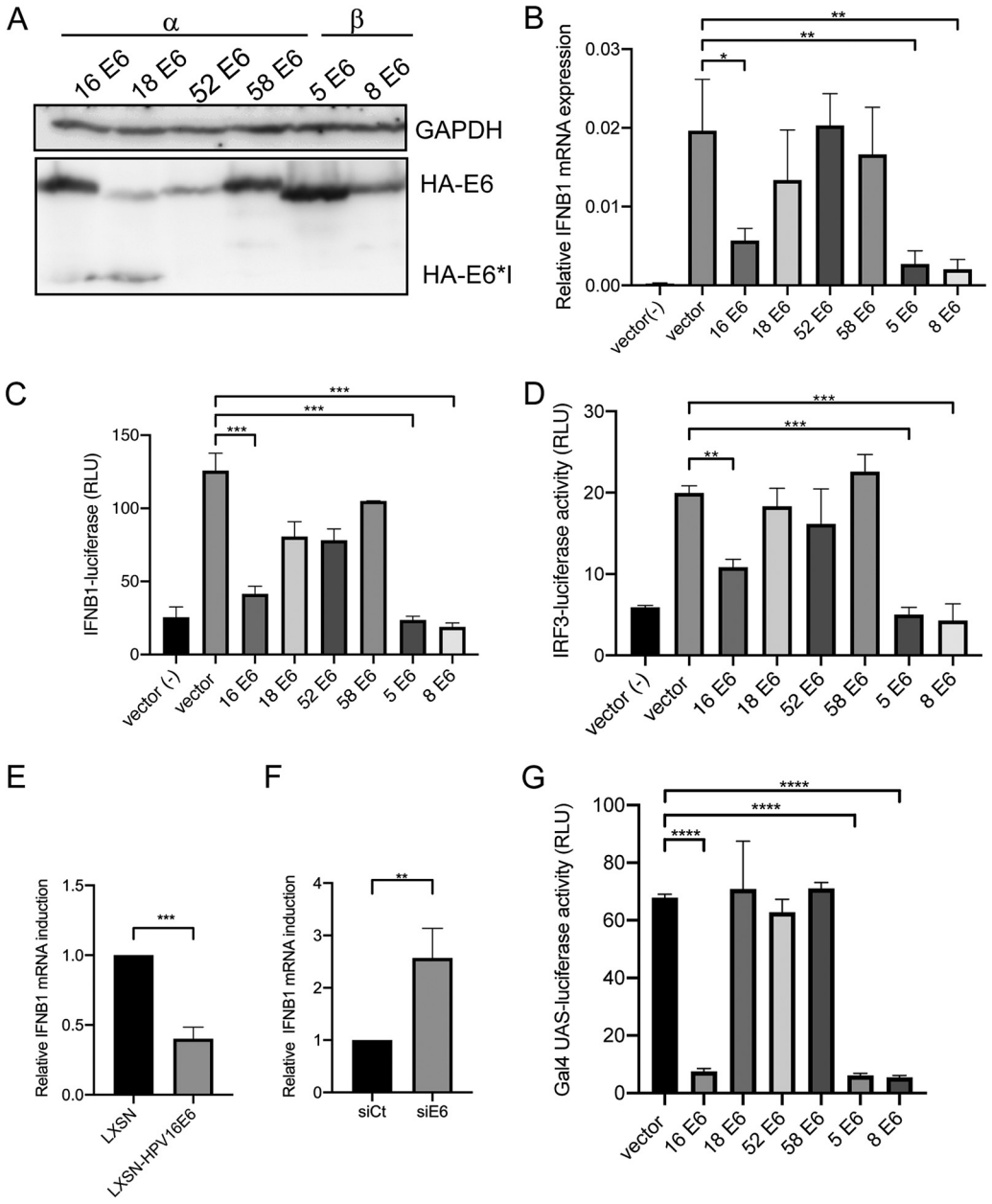

FIG 1 Inhibition of IRF3-driven IFNB1 mRNA expression by HPV16, HPV5, and HPV8 E6 proteins. (A) HEK293T cells were transfected with empty vector (pXJ-Flag-HA) or pXJ-Flag-HA-E6 plasmids (HPV 16, 18, 52, 58, 5, and 8 E6) and pFlag-RIG1. After 24 hours, cells were infected with Sendai virus (SeV) for 6 hours. Total proteins were extracted and analyzed by Western blotting for HA-E6 expression using anti-HA antibodies. (B) Total RNA was isolated and processed for IFNB1 mRNA expression by RT-qPCR. Results were expressed as mean ± SD of relative IFNB1 mRNA expression after normalization of samples with GAPDH mRNA expression. *, $P < 0.05$; **, $P < 0.01$; ***, $P < 0.001$. (C, D) HEK293T cells were transfected with pXJ-Flag HA-E6 plasmids, pFlag-RIG1 and the reporter plasmids, pIFN-β-Firefly luciferase plasmid (C) or pIRF3-firefly luciferase (D), and pTK-*Renilla* luciferase as the normalization plasmid. Twenty-four hours after transfection, cells were infected for 6 hours with SeV and then analyzed for luciferase activities. Cells transfected with empty vector and not infected with SeV (vector-) were used as negative controls. Results are expressed as the ratio between Firefly luciferase and *Renilla* luciferase. Results are expressed as mean ± SD and are representative of three independent experiments. (E) Human foreskin keratinocytes (HFKs) with empty vector (LXSN) or expressing the HPV16 E6 oncogene (LXSN-HPV16 E6) were infected for 6 hours with SeV. Total RNA was isolated and processed for IFNB1 mRNA expression and 18S mRNA for normalization. Results represent mean ± SD of three independent experiments. (F) SiHa cells were transfected with control siRNA (siCt) or siRNA targeting HPV16 E6 (siE6) at 28 nM for 48 hours. Cells were then infected for 6 hours with SeV. Total RNA was isolated and processed for IFNB1 mRNA expression and GAPDH mRNA for normalization. Results represent mean ± SD of three independent experiments. (G) Plasmid encoding GAL4 DBD-IRF3 ΔDBD and pXJ-Flag HA E6, the reporter plasmid pGal4 UAS-luciferase, and pTK-*Renilla* luciferase were transfected into HEK293T cells. After 24 hours of transfection, cells were analyzed for luciferase activities. Results were expressed as mean ± SD; *, $P < 0.05$; **, $P < 0.01$; ***, $P < 0.001$; ****, $P < 0.0001$.

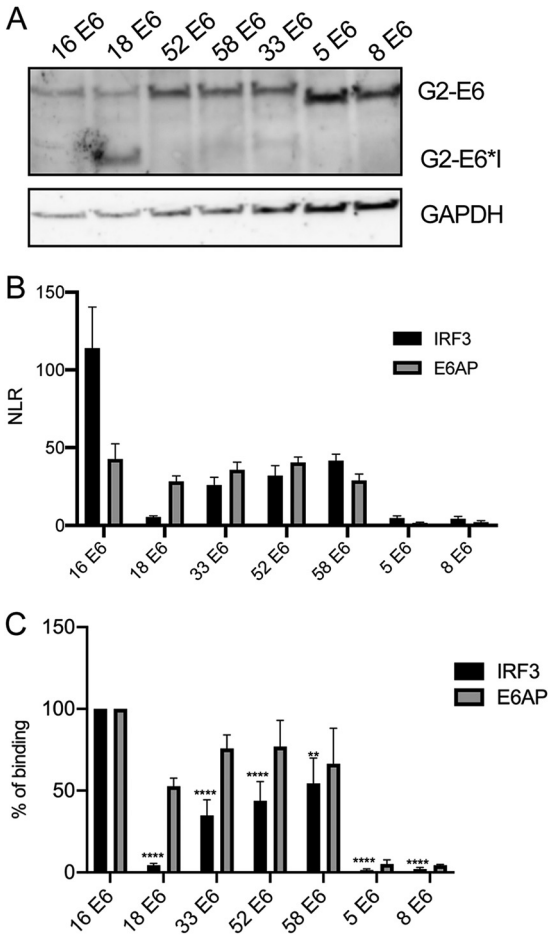

FIG 2 Analysis of the binding of E6 proteins to E6AP and IRF3. (A) HEK293T cells were cotransfected with plasmids encoding either HPV16, 18, 52, 58, 33, 5, or 8 E6 proteins fused to the G2 fragment of *Gaussia princeps* luciferase. After 24 hours of transfection, total proteins were analyzed by Western blotting for G2-E6 expression by using anti-Gluc antibodies. GAPDH expression was used as a loading control. (B) HEK293T cells were transfected with a plasmid encoding the E6 protein fused to the G2 fragment and a plasmid encoding IRF3 or E6AP fused to the G1 fragment of *Gaussia princeps* luciferase. Interactions between protein pairs were measured by using GPCA. Normalized ratio of luminescence (NLR) values were represented. Results from one representative experiment are expressed as mean ± SD. (C) GPCA results from 4 independent experiments were represented as % of binding by using HPV16 E6 as the reference. *, $P < 0.05$; **, $P < 0.01$; ***, $P < 0.001$; ****, $P < 0.0001$.

indicating a strong direct interaction between HPV16 E6 and IRF3. We then mapped the binding site of HPV16 E6 on the IRF3 protein. The IRF3 protein contained a DNA-binding domain (DBD), a transactivation domain containing the IAD (IRF association domain), and a signal response domain (SRD) containing serine residues that are phosphorylated by TBK1 upon activation (Fig. 3A). By using different IRF3 truncated constructs in the GPCA assay, HPV16 E6 was found to interact with the 1 to 150 amino acid region of IRF3, whereas there was no binding to the 1 to 113 amino acid region of IRF3 (Fig. 3B). These results suggest that the E6-binding site of IRF3 is located within the 113 to 150 amino acid region. This region contains an LxxLL motif (residues 140 to 144) that might fit within the HPV16 E6 hydrophobic pocket (26). Point mutations of leucine residues within the LxxLL motif of IRF3 (L140G/L143G/L144G) abolished the interaction with HPV16 E6 (Fig. 3B).

Binding of HPV16 E6 to LxxLL peptides. As shown above, the HPV16 E6 protein bound to both E6AP and IRF3, whereas HPV18 E6 bound to E6AP only. This finding was particularly intriguing since the LxxLL motifs displayed quite similar sequences, i.e.,

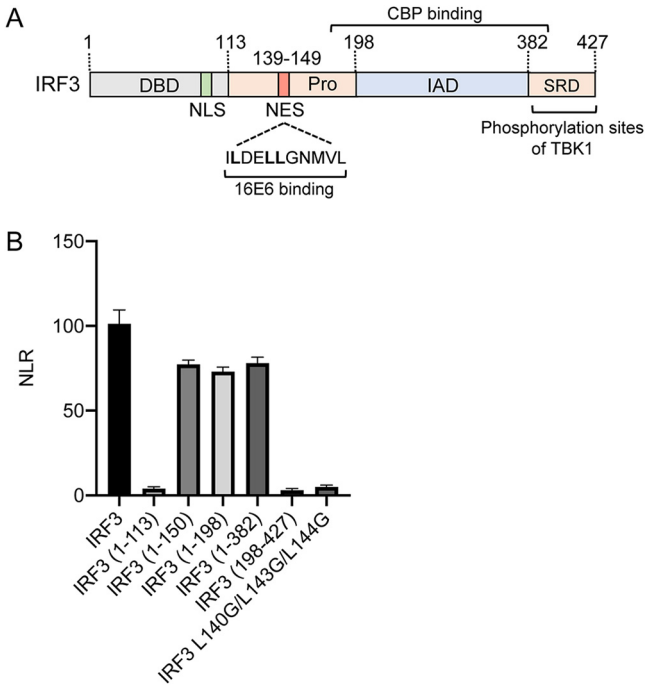

FIG 3 Mapping of the HPV16 E6 binding site on IRF3. (A) Schematic representation of domain organization of human IRF3 protein. DBD, DNA-binding domain; NES, nuclear export signal; NLS, nuclear localization signal; IAD, IRF activation domain; SRD, signaling response domain. (B) HEK293T cells were cotransfected with a plasmid encoding the HPV16 E6 protein fused to the G2 fragment and a plasmid encoding IRF3 full-length or IRF3 truncated forms or IRF3 L140G/L143G/L144G mutant fused to the G1 fragment. Interactions between protein pairs were measured by using the split *Gaussia princeps* luciferase complementation assay (GPCA). NLR values were represented. Results are expressed as mean ± SD and are representative of three independent experiments.

EDILDELLGNMV (IRF3) and ELTLQELLGEER (E6AP). This result suggests that the hydrophobic pocket of E6 proteins can adapt only specific LxxLL motifs and that the residues surrounding the LxxLL motif are crucial for the recognition. The interaction of the HPV16 E6 protein with LxxLL peptides was assessed by two independent binding approaches, namely, surface plasmon resonance (SPR) and holdup assay (29). The LxxLL motifs were carried by four biotinylated peptides, with two being derived from wild-type IRF3 and E6AP, and the other two bearing swapped chimeric sequences, chim-IRF3-E6AP (EDILDELLGEER) and chim-E6AP-IRF3 (ELTLQELLGNMV). In SPR experiments (Fig. 4A), the biotinylated peptides served as ligands and were fixed independently on the surface of the Biacore sensorchip, while the analyte was the purified recombinant maltose binding protein (MBP)-HPV16 E6 used at a constant 720 nM concentration. The normalized SPR signals for the four immobilized peptides reached an equilibrium as seen by a plateau visible at the end of the association phase (Fig. 4A). SPR experiments showed that HPV16 E6 had a higher relative affinity for chim-IRF3-E6AP or IRF3 peptides than chim-E6AP-IRF3 or E6AP peptides. To validate the SPR results, we used the holdup assay as an orthogonal approach. Holdup is a chromatographic retention method developed to analyze protein/peptide interactions in the medium-to-low binding strength range (29, 30). The holdup output is binding intensity (BI) (31) that is determined from the electropherograms obtained for the recombinant MBP-HPV16 E6 protein with the four peptides. The BI values obtained by holdup and the corresponding normalized equilibrium signals obtained by SPR were plotted as histograms for HPV16 E6 (Fig. 4B). Both approaches demonstrated that HPV16 E6 bound more strongly to IRF3 and chim-IRF3-E6AP peptides and weakly to E6AP and chim-E6AP-IRF3.These results highlight the importance of the residues at the N terminus and at the x position within the LxxLL motif of IRF3 (EDI**L**DE**LL**) for binding to HPV16 E6.

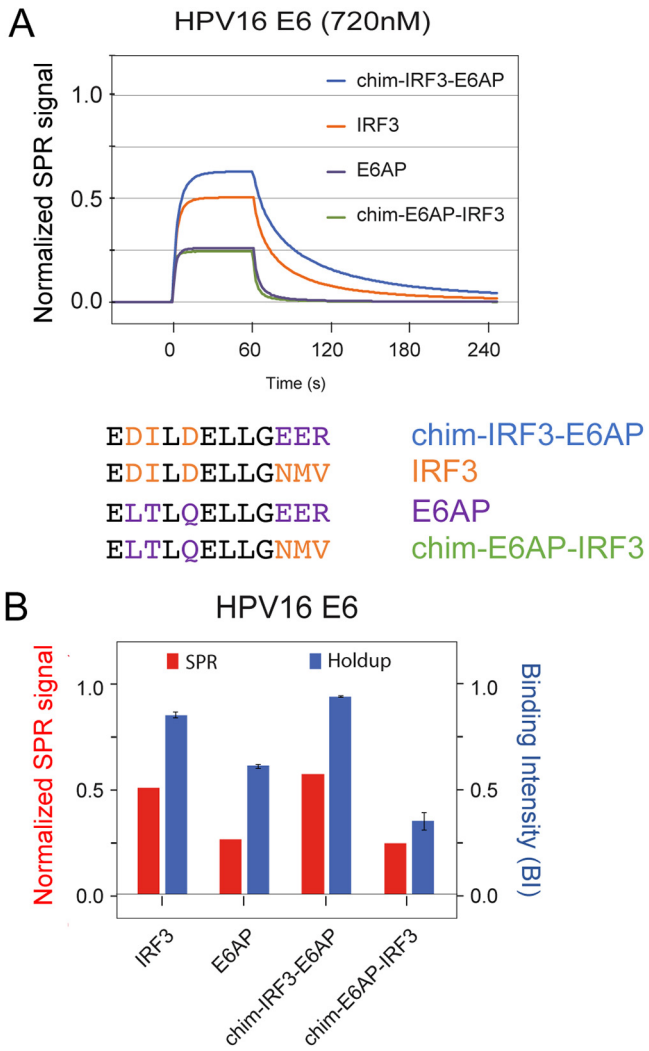

FIG 4 Interactions between HPV16 E6 and LxxLL peptides analyzed by SPR and Holdup. (A) Representative sensorgrams recorded by surface plasmon resonance resulting from the interaction between the HPV16 E6 protein (injected at a 720 nM concentration) and the different IRF3, E6AP, or chimeric peptides. Binding curves display normalized SPR signal as a function of time (see Materials and Methods). (B) The steady-state values extracted by averaging the signal in a 5-second window at the end of the association phase are compared with the binding intensity (BI) obtained by holdup assay for the same peptides interacting with HPV16 E6. Error bars on BI correspond to the standard deviations of triplicated data.

Crystallographic structure of HPV16 E6 in complex with the IRF3-LxxLL peptide. In order to better understand the HPV16 E6/IRF3 interaction, we crystallized and solved the structure of the complex. We employed a similar strategy to that used previously to solve the structure of the HPV16 E6/E6AP-LxxLL peptide complex (6). Shortly, a purified HPV16 E6 (F47R, 4C/4S) protein was mixed with an equimolar amount of purified MBP-IRF3-LxxLL fusion. The complex yielded crystals that diffracted at a resolution of 1.5 Å. The structure was solved by molecular replacement using the known structures of MBP and HPV16 E6 as a template (Table 1). The crystallographic structure of the HPV16 E6/IRF3-LxxLL complex (PDB 6SJA) is shown in Fig. 5A. In agreement with the previous HPV16 E6/E6AP-LxxLL structure (PDB 4GIZ), the overall fold of E6 consisted of two zinc-binding domains (named E6N and E6C) connected by a linker helix. As expected, the IRF3 peptide localized within the hydrophobic pocket of E6 as described before for the E6AP peptide (6).

The isolated E6 zinc-binding domains (E6N and E6C) in the E6/IRF3 and E6/E6AP complexes were almost superimposable, with a root mean square deviation (RMSD) of

TABLE 1 X-ray diffraction data collection and refinement statistics

Parameter	Data[a] for HPV16-E6 + MBP-IRF3-LxxLL
Data collection	
Beamline	Swiss Light Source X06DA
Detector	Dectris Pilatus 2M
Wavelength (Å)	0.900000
Space group	P 21 21 2
Space group no.	18
Cell dimensions	
a, b, c (Å)	97.66, 132.87, 43.03
α, β, γ (°)	90, 90, 90
Solvent fraction, V_M (Å^3/Da)	0.47, 2.33
Wilson B-factor (Å^2)	19.2
Mosaicity (Å)	0.26
Resolution (Å)	50.0–1.50 (1.59–1.50)
No. of observed reflections	1,193,086 (180,666)
No. of unique reflections	170,435 (26,948)
R_{meas} (%)	7.4 (124.7)
R_{sym} (%)	6.8 (115.0)
$I/\sigma(I)^{asymptotic}$	26.63
$I/\sigma(I)$	15.95 (1.65)
$CC_{1/2}$	99.9 (61.8)
Completeness (%)	98.1 (95.7)
Redundancy	7.0 (6.7)
Refinement	
Resolution (Å)	45.833–1.499
No. of reflections	89,009 (8,511)
R_{work}/R_{free}	15.90/19.05 (26.69/29.71)
No. of TLS groups	none
B-factor refinement	Anisotropic except for H and HOH
No. of atoms	4,668
B-factors, isotropic (*n*)	
Protein	4,124
Ligands	58
Water	486
Protein	28.2
Ligands	28.9
Water	37.6
Geometry	
RMSD bond lengths (Å)	0.007
RMSD bond angles (°)	0.88
Ramachandran preferred (%)	
Preferred	98.44
Allowed	1.56
Outliers	0.00

[a]Values in parenthesis are for highest resolution shell.

0.46 Å for E6N and 0.34 Å for E6C. However, when the full-length proteins in both complexes were aligned, the position of E6C relative to E6N was shifted (Fig. 5B). By subtracting the solvent accessible surface area (SASA) per residue of the E6 molecule in the crystal structure in absence and presence of the LxxLL peptide, we identified the residues involved in the interaction (Fig. 5C and D). The hydrophobic contacts mainly in charge of the LxxLL motif recognition were well conserved with respect to that previously reported for E6AP LxxLL recognition (V31, Y32, L50, V53, V62, L67, Y70, R102, Q107, and R131) (6), (Fig. 5D). In addition, several contacts were specific to each complex and may allow E6 to discriminate between the different LxxLL motifs. Interestingly, many of the different interactions involved the same E6 residues playing different physicochemical roles (highlighted in Fig. 5D), which may allow E6 to adapt to different partners. In the E6/IRF3 complex, the main differences comprised a novel

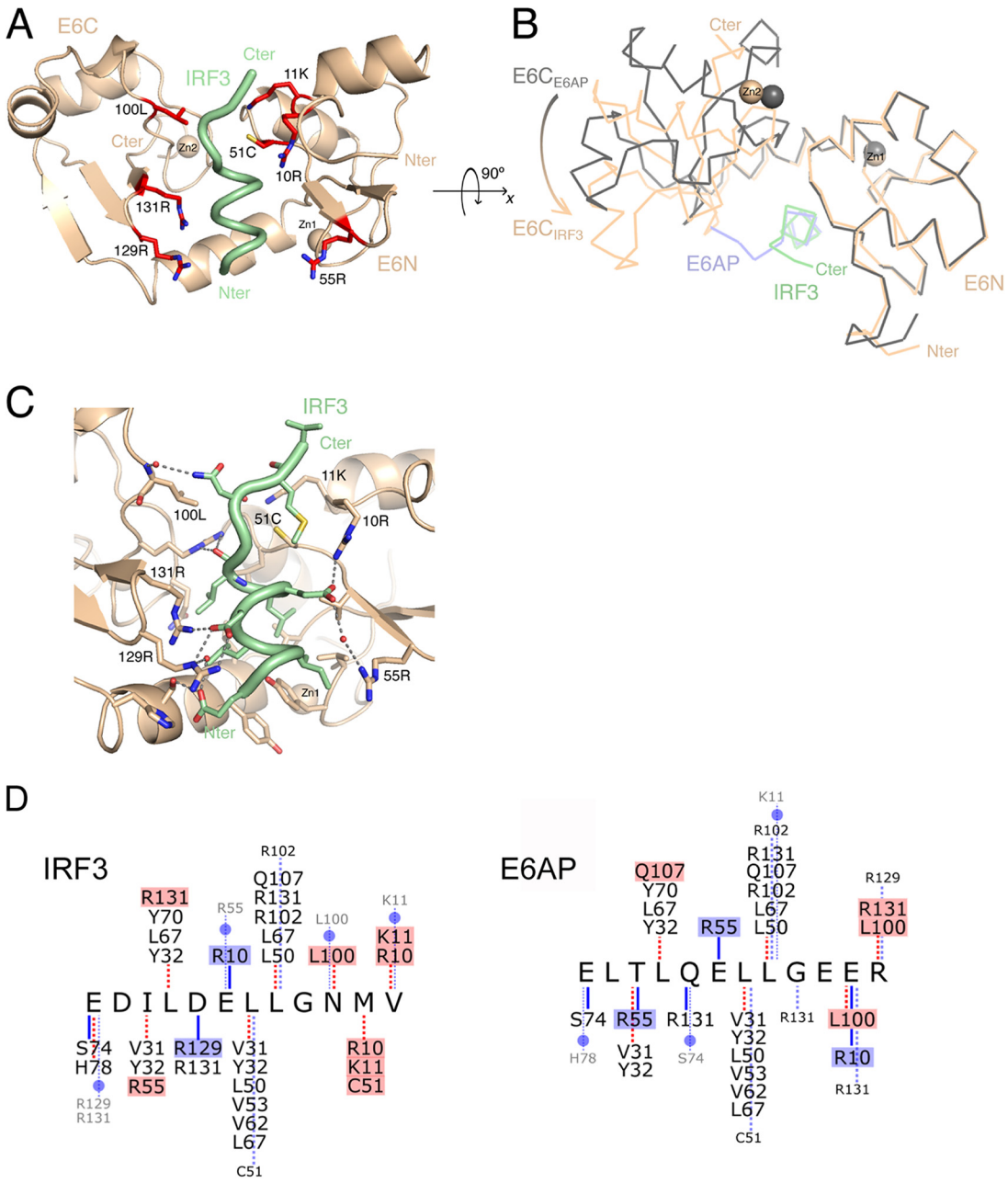

FIG 5 Crystallographic structure of the HPV16 E6/IRF3-LxxLL peptide complex. (A) Crystallographic structure of HPV16 E6 and LxxLL peptide of IRF3. Wheat, HPV16 E6; green, IRF3-LxxLL; spheres, Zn (II). The structure has been deposited in the PDB and is available under accession number 6SJA. (B) Superposition of the crystallographic structures of the HPV16 E6 (gray)/LxxLL-E6AP (blue) (PDB 4GIZ) and HPV16 E6 (wheat)/LxxLL-IRF3 (green) complexes. (C) Detail of the hydrophobic pocket of HPV16 E6 in complex with IRF3-LxxLL; interacting residues are represented in sticks. (D) Contacts residues between IRF3 peptide or E6AP peptide (6) and HPV16 E6 protein. Bottom, all contacts between E6 and LxxLL peptides. Red dashed lines, hydrophobic contact; blue continuous lines, direct polar contacts through side chain; blue dashed lines, polar contacts through main chain; blue dashed lines with circle, polar contacts mediated by water molecule. Squared residues are unique contacts compared with E6AP recognition.

polar contact through R129, a shift in the interaction through R10, and a novel hydrophobic contact through C51. These specific contacts may explain the lack of affinity of HPV18 E6 for IRF3-LxxLL since those residues were not conserved in the HPV18 sequence where they were replaced by A131, Y12, and F53, respectively. These observations are in agreement with computational simulations of the HPV16 E6/IRF3-LxxLL complex, which pointed to R10, C51, and R129 as the main contributors to the free energy of binding (Fig. 6).

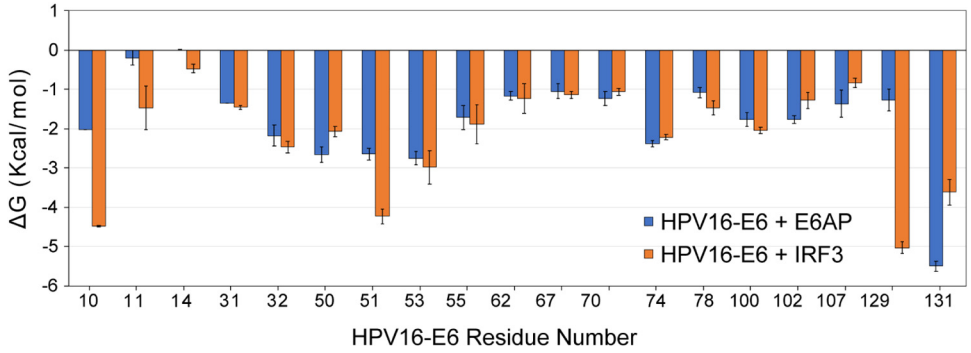

FIG 6 Free energy of binding per residue of HPV16 E6 in complex with IRF3-LxxLL and E6AP-LxxLL motives. Free energy was calculated on a set of structures representing the conformational space sampled during MD simulations of the X-ray complexes devoid of MBP. The binding free energy (ΔG) is estimated from the equation $\Delta G = \Delta G^{vdw} + \Delta G^{elec} + \Delta G^{elec}_{solv} + \Delta G^{np}_{solv}$ where ΔG^{vdw} and ΔG^{elec} are the van der Waals and electrostatic contributions associated with complex formation, whereas ΔG^{elec}_{solv} and ΔG^{np}_{solv} are the electrostatic and nonpolar contributions related to solvation.

Based on our structural data and sequence alignment of E6 from HPV16, HPV52, HPV58, HPV33, and HPV18 types, we mutagenized some critical residues within the HPV16 E6 protein implicated in the binding to IRF3. The expression level of the different G2-E6 mutants (K11T, C51T, L50E, R10Y, R129A, and R10Y/R129A) was verified by Western blotting (Fig. 7A), and the E6 mutants were tested for binding to E6AP or IRF3 by GPCA (Fig. 7B). The R10Yand R129A mutations decreased slightly the binding to E6AP, whereas the mutations K11T and C51T had no effect. The mutation into E of the highly conserved L50 residue completely abolished the binding to E6AP as published (6) and the binding to IRF3. The R129A mutant and the R10Y/R129A double mutant were partially impaired for IRF3 binding and E6AP binding, with a more pronounced effect on IRF3 binding. The R129 and R10 residues of HPV16 E6 were found to be in contact with D141 and E142 residues of IRF3 ($_{137}$EDIL**DE**LLGNMV$_{148}$) in the crystal structure. This result was in agreement with the SPR and holdup data as well as with the free energy of binding computations. The impact of HPV16 E6 mutants on IFN-β1 expression was studied in HEK293T cells transduced with Sendai virus particles. HPV16 E6 R129A and R10Y/R129A mutants inhibited moderately the IFN-β (IFNB1) mRNA expression, whereas the HPV16 E6 L50E mutant did not inhibit IFN-β expression (Fig. 7C). The other E6 mutants (R10Y, K11T, and C51T) inhibited IFNB1 expression in a similar manner as the HPV16 E6 wild type. In conclusion, the inhibition of IFN-β mRNA expression by HPV16 E6 seems to be correlated with its IRF3 binding activity.

Impact of the HPV16 E6 protein on IRF3 phosphorylation and dimerization. To understand the molecular mechanism of inhibition of IFN-β mRNA expression by E6 proteins, the upstream signaling cascade was explored. Upon signal transduction, TBK1 is activated by phosphorylation on its S172 residue and then, in turn, activated TBK1 phosphorylates IRF3 on serine residues in its SRD domain (such as S396) (32). In HEK293T cells expressing HPV16 or HPV8 E6 and infected with Sendai virus, total proteins were analyzed by Western blot for TBK1 and IRF3 expression and phosphorylation. The level of phosphorylated p-S172 TBK1 was the same in HPV16 E6, HPV8 E6, or control cells (Fig. 8A). In contrast, we observed a decrease of phosphorylated pS396 IRF3 levels when HPV16 E6 was expressed (Fig. 8A). The phosphorylation of IRF3 by TBK1 induces a conformational change allowing the IRF3 dimerization and its translocation into the nucleus (33). To analyze IRF3 dimer formation, total proteins were loaded on a native gel (Fig. 8B). Monomers or dimers of IRF3 were detected by Western blot using an anti-IRF3 antibody. In agreement with the decrease of phosphorylated p-S396 IRF3 levels, there was less IRF3 dimer formation in cells expressing HPV16 E6 (Fig. 8B). In contrast, expression of HPV8 E6 did not induce any change in IRF3 phosphorylation or dimerization.

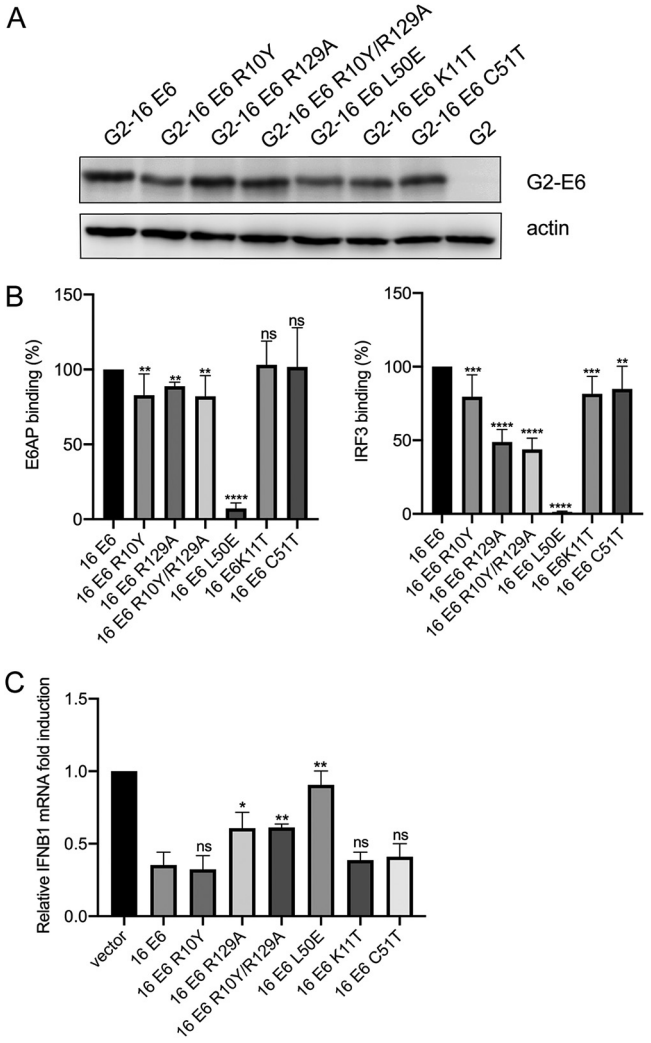

FIG 7 An analysis of HPV16 E6 mutants defective for IRF3 binding. (A) HEK293T cells were transfected with a plasmid encoding HPV16 E6 wild-type or mutant (R129A, R10Y/R129A, R10Y, L50E, K11T, and C51T) fused to the G2 fragment of *Gaussia princeps* luciferase. Total proteins were analyzed by Western blotting using anti-Gluc antibodies. Actin expression was used as a loading control. (B) HEK293T cells were transfected with a plasmid encoding HPV16 E6 wild-type or mutant fused to G2 fragment and a plasmid encoding IRF3 or E6AP fused to the G1 fragment. Interactions between protein pairs were measured using GPCA. Results are shown as % of binding using the HPV16 E6 wild type as the reference (n = 4 individual experiments). (C) HEK293T cells were cotransfected with pFlag-RIG1 and pXJ-Flag-HA or pXJ-Flag-HA-16E6 wild-type or mutants (R10Y, R129A, R10Y/R129A, L50E, K11T, and C51T). Twenty-four after transfection, cells were infected for 6 hours with SeV. Total RNA was extracted and processed for IFNB1 mRNA expression by using RT-qPCR. Results were expressed as mean ± SD (n = 3 independent experiments). IFNB1 relative mRNA expression after normalization of samples with GAPDH mRNA expression is shown. *, $P < 0.05$; **, $P < 0.01$; ***, $P < 0.001$; ****, $P < 0.0001$; ns, not significant.

Binding of HPV5 and HPV8 E6 proteins to the IBiD domain of CBP. Upon translocation into the nucleus, activated IRF3 dimers recruit the coactivators CBP/p300 to stimulate chromatin acetylation and IFN-β (IFNB1) gene expression (12, 34, 35). More precisely, the IRF3 fragment spanning residues 174 to 394 forms a complex with a 46-residue segment within the C-terminal glutamine-rich region of CBP, named the IRF3-binding domain (IBiD) (36, 37). Notably, HPV16 E6 protein binds to CH1, CH3, and C-terminus regions of p300 and its paralog CBP (38). HPV5 and HPV8 E6 proteins interact with p300 and can induce its degradation, whereas they do not induce the degradation of CBP (39). We probed the interaction of the IBiD of CBP, with either full-length IRF3 or the IRF3 construct (residues 173 to 393) by using GPCA (Fig. 9A). The IBiD of CBP induced a higher GPCA signal with the IRF3

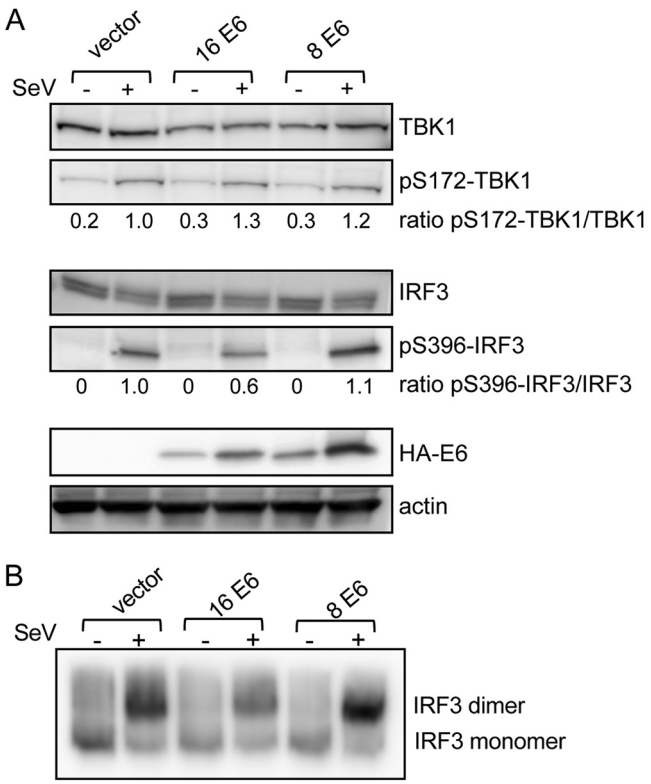

FIG 8 Inhibition of IRF3 phosphorylation and dimerization by expression of HPV16 E6. (A) HEK293T cells were transfected with pFlag-RIG1 and pXJ-Flag-HA (vector) or pXJ-Flag-HA-16E6 or pXJ-Flag-HA-8E6. Twenty-four hours after transfection, cells were infected with (+) Sendai virus for 6 hours. Cleared cellular lysates were analyzed by Western blotting for TBK1 and IRF3 expression and phosphorylation. The intensities of protein bands for IRF3, pS396 IRF3, TBK1, and pS172 TBK1 were quantified using ImageJ. The ratios pS396-IRF3/IRF3 and pS172TBK1/TBK1 were shown. The figure was representative of four independent experiments. (B) Cleared cellular lysates (as in A) were loaded on an 8% native gel. The presence of monomers or dimers of IRF3 was detected by using an anti-IRF3 antibody.

fragment (residues 173 to 393) than with the full-length IRF3. This result might be explained because the shorter construct lacks the inhibitory sequence within the C terminus of IRF3. Surprisingly, we found that the HPV8 and HPV5 E6 proteins interacted with the IBiD domain of CBP in contrast to E6 proteins from α-genus HPV types (Fig. 9A). To confirm the GPCA results, we performed a GFP-trap experiment by transfecting HEK293T cells with pC1-eGFP-IBiD, p3xFlag-IRF3 5S/D and p3xFlag-HPV16 E6, or p3xFlag-HPV8 E6 plasmids. The phosphomimic mutant IRF3 5S/D is a constitutively active mutant of IRF3. We found that GFP-IBiD interacted with IRF3 5S/D or HPV8 E6, whereas HPV16 E6 did not interact directly with the IBiD domain (Fig. 9B). In HEK293T cells transduced by Sendai virus particles, overexpressed Flag-CBP was able to immunoprecipitate the HPV16 E6 protein and to a larger extent the HPV8 E6 protein (Fig. 9C). Moreover, the expression of the HPV8 E6 protein decreased the recruitment of phospho-S396 IRF3 on CBP. This result suggests that the HPV8 E6 protein might compete with IRF3 for the binding to the IBID domain of CBP. This interaction might explain the inhibition of IFN-β1 expression by the HPV8 E6 protein (and most likely by HPV5 E6 protein as well).

DISCUSSION

To overcome the host type I interferon (IFN) response, viruses have evolved diverse strategies by (i) interfering with DNA or RNA sensors, (ii) inhibiting the TBK1/IκB kinase ε (IKKε) activity, (iii) binding directly to IRF3, (iv) increasing IRF3 degradation, (v) inhibiting the recruitment of CBP/p300 at type I IFN gene promoters, (vi) competing with IRF3 for binding to CBP/p300, and (vii) inhibiting the JAK-STAT pathway (40). To induce

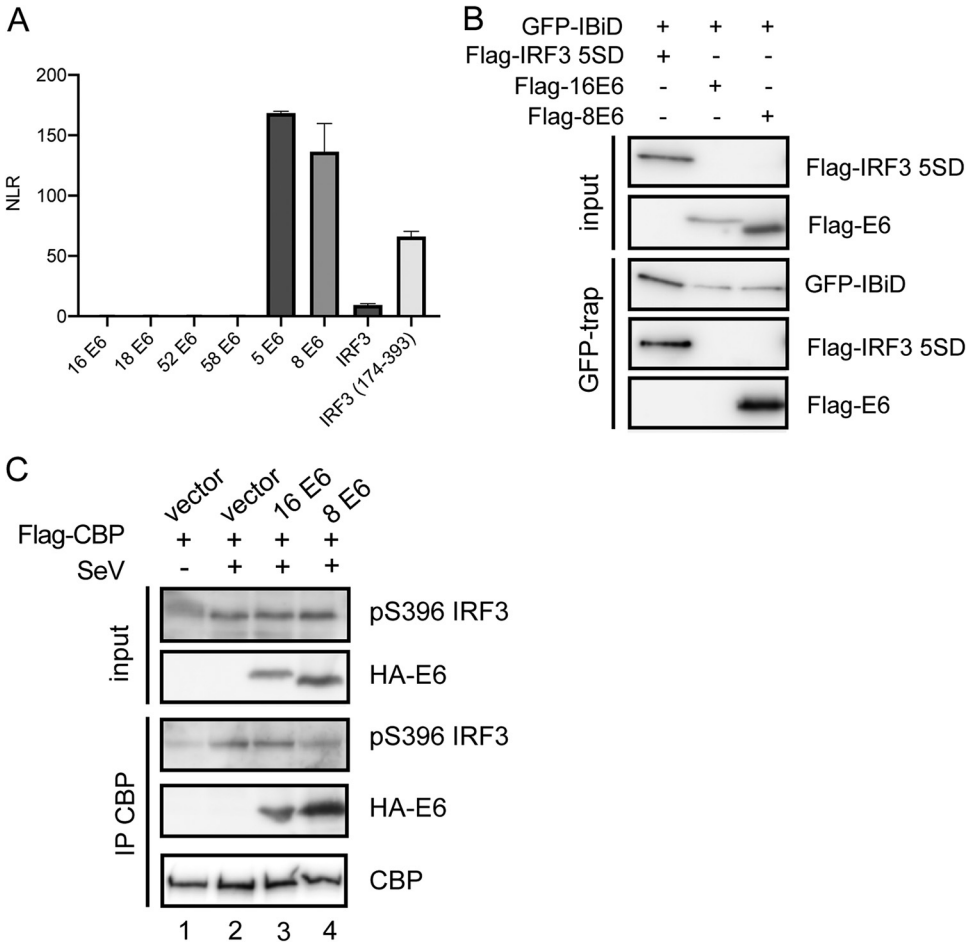

FIG 9 Binding of HPV5 and HPV8 E6 to the IBiD domain of CBP. (A) HEK293T cells were transfected with a plasmid encoding G1-IBiD$_{(2066\text{-}2111)}$ and a plasmid encoding G2-IRF3 or G2-IRF3$_{(174\text{-}393)}$ or G2-E6 from different types (HPV16, HPV18, HPV52, HPV58, HPV5, and HPV8). After transfection, GPCA was performed and NLR for each pair was represented. (B) HEK293T cells were cotransfected with pC1-eGFP-IBiD$_{(2017\text{-}2111)}$, p3xFlag-IRF3 5S/D, p3xFlag-HPV8 E6, or p3xFlag-HPV16 E6 plasmids. Twenty-four hours after transfection, cleared cellular lysates were incubated with anti-GFP magnetic beads. Proteins in the lysates (input) and proteins retained on anti-GFP magnetic beads were analyzed by Western blotting using anti-Flag and anti-GFP antibodies. (C) HEK293T cells were cotransfected with pFlag-CBP and pXJ-Flag-HA, pXJ-Flag-HA-16E6, or pXJ-Flag-HA-8E6. Twenty-four hours after transfection, cells were infected with (+) or without (−) Sendai virus for 6 hours. Proteins from cleared lysates were immunoprecipitated with anti-CBP antibodies. Retained proteins on protein G-beads were analyzed by Western blot using an anti-phospho(pS396) IRF3 antibody and anti-HA antibody.

persistent infection, human papillomaviruses escape the innate immune response by expressing dedicated early viral proteins (E2, E6, and E7). In this work, we have investigated the effect of HPV E6 proteins from different genus types (mucosal high-risk α-type and cutaneous β-type) on the IFN-β (IFNB1) gene expression. High-risk mucosal α-type HPVs are associated with cervical cancers, anogenital cancers, and a subset of head and neck squamous cell carcinoma (HNSCC). HPV16 is the most prevalent HPV and accounts for 50% of cervical cancers and 90% of oropharyngeal cancers. HPVs of β-genera include more than 54 types which are subdivided into 5 subfamilies (β1 to β5) (41). HPV5 and HPV8 types belong to the HPV-β1 family and are considered possible etiological agents (carcinogen group 2B) of cutaneous SCC in immunosuppressed *Epidermodysplasia verruciformis* individuals (42).

We found that HPV16 E6 and HPV8 (or HPV5) E6 proteins employ distinct strategies to interfere with the IRF3-dependent IFN-β response (Fig. 10). The HPV16 E6 protein is a strong binder of the IRF3 transcription factor, whereas HPV5 and HPV8 E6 proteins interact with the IRF3-binding domain (IBiD) of the transcriptional coactivator CBP. The

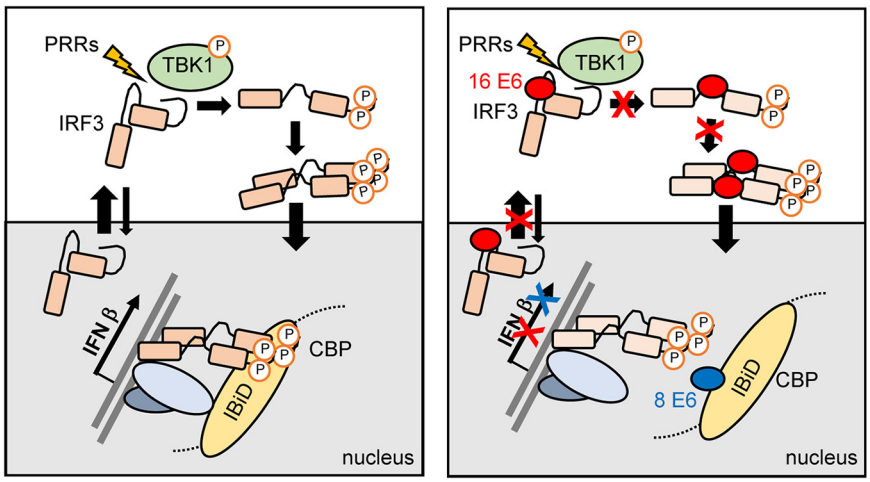

FIG 10 Strategies employed by HPV16 and HPV8 E6 proteins to interfere with IRF3-mediated IFN-β expression. Upon stimulation with pathogen-associated molecular patterns (PAMPs), pattern recognition receptors (PRRs) activate the TBK1 kinase and recruit the transcription factor IRF3, which is localized in a latent form in the cytoplasm. Activated TBK1 phosphorylates the C terminus part of IRF3, leading to a conformation change that allows IRF3 dimerization. IRF3 dimers translocate into the nucleus and interact with the transcription factors IRF7, ATF2/c-Jun, and NF-κB and the cofactor CBP to form the IFN-β enhanceosome. The latter one binds to the IFN-β enhancer and activates the IFN-β1 (IFNB1) gene transcription. The HPV16 E6 protein binds directly to IRF3 and interferes with its phosphorylation by TBK1 and/or its nuclear export and its transactivation activity. In contrast, HPV8 (HPV5) E6 binds to the IBiD domain of CBP and competes with IRF3 for CBP interaction. By targeting IRF3 and CBP, HPV16 and HPV8 E6 proteins, respectively, inhibit IFN-β expression.

transcriptional coactivator CBP and its paralog p300 are known to interact with more than 400 partners, including the basal transcription machinery and numerous transcription factors and to acetylate proteins, such as histones and p53. CBP/p300 are also targeted by HPV proteins. Indeed, high-risk α-type HPV E6 proteins are able to interact with p300 and to inhibit p300-dependent p53 acetylation (43–45). Cutaneous β1-type HPV5 and HPV8 E6 proteins induce the proteasome-dependent degradation of p300 by blocking the p300/AKT association (39). Here, we demonstrate that HPV5 and HPV8 E6 proteins can interact with the IRF3-binding domain of CBP, called IBiD or nuclear coactivator binding domain (NCBD). The IBiD interacts with a hydrophobic surface of IRF3, which in latent form is covered by autoinhibitory elements (37). The IBiD is targeted by cellular proteins (such as p53, IRF3, and ACTR) or viral proteins (such as Adenovirus E1A-12S and KSHV-IRF1) and can adopt different conformations depending on the identity of its partner (36). By binding to the IBiD, HPV5 and HPV8 E6 might compete with IRF3 for a CBP interaction, explaining their ability to inhibit IFN-β gene expression.

We demonstrated that the HPV16 E6 protein binds to a 12-amino acid LxxLL motif (residues 137 to 148), localized in a flexible linker between the DNA-binding domain (DBD) and the IRF association domain (IAD) of IRF3. As shown by our X-ray data, the LxxLL motif of IRF3 docks into the hydrophobic pocket of E6, like the LxxLL motif of E6AP (6), although at the expense of a repositioning of the E6-C domain. The LxxLL motifs of E6AP and IRF3 are very similar, so it is puzzling why HPV16 E6 can bind to IRF3 and E6AP, whereas HPV18 E6 binds only to E6AP. Our SPR, holdup, X-rays, and mutagenesis data highlighted the importance of residues D and E within the LDELL motif of IRF3 to make specific contacts with HPV16 E6 residues (R10 and R129). In HPV52, HPV33, and HPV58 E6 proteins, the R10 residue is conserved but not the R129 residue. In contrast, neither of these two residues are in HPV18 E6 (corresponding to Y12 and A131), explaining at least in part the absence of binding to IRF3. We found that in HEK293T cells infected with Sendai virus, HPV16 E6 expression decreased the level of IRF3 phosphorylation by TBK1. In addition, the Gal4-IRF3 reporter assay

experiment suggested that HPV16 E6 might inhibit the transcriptional activity of IRF3. As the HPV16 E6 binding site is located in the flexible linker that contains autoinhibitory elements (46, 47) and overlaps with the nuclear export signal (NES) of IRF3 (48), binding of E6 might alter the conformation of IRF3 in a way that it could impair its phosphorylation by TBK1, its export from the nucleus to the cytoplasm, and/or its transactivation activity. Several studies have demonstrated proapoptotic functions of IRF3 in virus-induced apoptosis and DNA damage response (49–51). Therefore, how and to what extent the HPV16 E6 protein interferes with the proapoptotic functions of IRF3 is an interesting issue to address.

This work highlights the remarkable versatility of E6 proteins which, despite a high overall sequence conservation across HPV species, have evolved to recognize either one or the other component of the IRF3-CBP complex. Among the high-risk mucosal HPVs, only HPV16 E6 interacts strongly with IRF3; this interaction might give a selective advantage to HPV16, explaining, in part, its high prevalence in HPV-associated cancers.

MATERIALS AND METHODS

Cell culture and viruses. HEK293T and SiHa cells were grown and maintained in Dulbecco's modified Eagle's medium (DMEM), supplemented with 10% fetal calf serum (FCS) at 37°C with 5% CO_2. Human foreskin keratinocytes (transduced with pLXSN empty-vector or pLXSN-HPV16E6) were obtained from D. Galloway (52). Keratinocytes were grown in EpiLife basal medium supplemented with 60 μM calcium chloride, bovine pituitary extract (0.2% vol/vol), recombinant insulin-like growth factor-I (0.01 μg/mL), hydrocortisone (0.18 μg/mL), bovine transferrin (5 mg/mL), and human epidermal growth factor (0.2 ng/mL). SeV-DI-H4 particles, obtained from Dominique Garcin (Medical Faculty, Geneva, Switzerland) were composed of complete Sendai virus (SeV) genomes and a large number of small, copyback defective interfering (DI) genomes, which are strong inducers of IFN-β gene transcription (53).

Antibodies, reagents, and plasmid constructs. Rabbit monoclonal antibodies against Phospho-(S396) IRF3 (PDB 4D4G), a polyclonal antibody against IRF3 (D6I4C), a rabbit antibody against CBP (D6C5), rabbit monoclonal antibodies against phospho-S172 TBK1/NAK (D52C2), and rabbit polyclonal antibodies against TBK1/NAK (D1B4) were purchased from Cell Signaling Technology. Mouse anti-GAPDH and anti-Flag M2 antibodies were purchased from Sigma-Aldrich. A mouse anti-GFP antibody was purchased from Roche. Rabbit anti-Gluc (Gaussia Luciferase) was purchased from New England BioLabs (NEB). GPCA vectors pSPICA-N1 and pSPICA-N2 (both derived from the pCiNeo mammalian expression vector) express the G1 and G2 complementary fragments, respectively, of the *Gaussia princeps* luciferase linked to the N-terminal ends of tested proteins via a flexible hinge polypeptide of 20 amino acid residues as described (27). The open reading frames (ORFs) encoding E6 proteins from different genotypes, the E6AP fragment (residues 291 to 875 of isoform II), and IRF3 proteins were amplified by PCR and cloned into vector $pDONOR_{207}$ by recombination cloning (Gateway system, Invitrogen). The resulting entry clones were then transferred into Gateway-compatible GPCA destination vector pSPICA-N1 or pSPICA-N2. The plasmids pFlag-TBK1, pFlag-CBP, and pIRF3-luciferase (containing PRD III binding sites) were given by Johanna L. Shisler. pIFN-β-luciferase (containing PRD I, II, III, and IV binding sites) and the p3xFlag-IRF3 5S/D (S396D, S398D, S402D, S405D, and T404D) construct were provided by Andrew Bowie, and pFlag-RIG1 was given by Damien Arnoult. The E6 sequences from HPV16, 52, 58, 18, 5, and 8 were inserted into a pSG5 puro-derived vector (pXJ-Flag HA). The pGal4 (DBD)-IRF3(ΔDBD) allows the expression of the DBD of Gal4 fused to the C-terminal region of IRF3 (residues 113 to 427, lacking its N-terminal DBD). The IBiD construct (2017-2111) was cloned into the pC1 plasmid (gift from Institut de Génétique et de Biologie Moléculaire et Cellulaire [IGBMC] cloning platform). Residues 137 to 149 of human IRF3 (peptide sequence, EDILDELLGNMV) were cloned at the C terminus of a mutant MBP after a three-alanine linker. The point mutations introduced in MBP (D83A, K84A, K240A, E360A, K363A, and D364A) have been described previously to increase the propensity of MBP to crystallize. The E6 4C/4S F47R mutant of HPV-16 was cloned into the pETM-41 vector containing an N-terminal His_6-MBP tag followed by a Tobacco Etch Virus (TEV) protease cleavage site.

Cell treatment, virus infection, and Western blot analysis. HEK293T cells were cotransfected by Lipofectamine 2000 with pXJ-FLAG-HA-16E6, 18E6, 52E6, 58E6, 5E6, and 8E6 plasmids and pFlag-RIG1 plasmids. Twenty-four hours after transfection, cells were infected with Sev-DI-H4 particles for 1 hour in serum-free DMEM (around 10^7 PFU/10^6 cells) and then incubated in complete DMEM for 5 hours. Cells were harvested and lysed in 50 mM Tris-HCl (pH 7.5), 150 mM NaCl, 1% Triton X-100, protease inhibitor cocktail (Roche), and phosphatase inhibitors (Phospho-STOP; Roche). After centrifugation, cleared lysates were analyzed by SDS-PAGE and Western-blot. SiHa cells were transfected by siRNAs at a 28 nM final concentration for 48 hours using Lipofectamine 2000. The siRNA negative control (siCt) was purchased from Horizon Discovery (siGenome nontargeting control siRNA pool 2). The siE6 targets the intronic sequence of HPV16 E6 (corresponding to nucleotide 385 to 403 of the bicistronic HPV16 E6/E7 transcript) and has the following sequences: 5′-CCGUUGUGUGAUUUGUUAAUU-3′ (sense) and 5′-UUAACAA AUCACACAACGGUU-3′ (antisense).

GPCA. HEK293T cells were seeded in a white 96-well plate at a concentration of 2.5×10^4 cells per well. After 24 hours, cells were transfected with 100 ng of pSPICA-N2 and 100 ng of pSPICA-N1. At 24 hours posttransfection, cells were washed with 50 μL of phosphate-buffered saline (PBS) and lysed with

40 μL of *Renilla* lysis buffer (Promega, E2820) for 30 min. *Gaussia princeps* luciferase enzymatic activity was measured using a Berthold Centro LB960 luminometer by injecting 50 μL per well of luciferase substrate reagent (Promega, E2820) and counting luminescence for 10 seconds. Results were expressed as normalized luminescence ratio (NLR). For a given protein pair, A/B, NLR = (G1-A + G2-B)/[(G1-A + G2) + (G1 + G2-B)] as described in reference 27.

GFP-Trap experiment. HEK293T cells were transfected with pC1-eGFP-IBiD$_{(2017\text{-}2111)}$, p3xFlag IRF3 5S/D and p3xFlag HPV8 E6, or p3xFlag HPV16 E6. Twenty-four hours after transfection, total proteins were extracted using lysis buffer, 50 mM Tris (pH 7.5), 150 mM NaCl, 1% Triton X-100, 0.5 mM EDTA, and protease cocktail inhibitors (Roche) for 30 minutes on ice. After being cleared by centrifugation, cellular lysates were incubated with anti-GFP magnetic beads (ChromoTek) overnight at 4°C. After several washes of the beads, protein complexes were eluted with SDS sample buffer and analyzed by Western blot.

Native PAGE. Native polyacrylamide gel electrophoresis was performed using an 8% native gel. Briefly, the gel was prerun with 25 mM Tris, 192 mM glycine (pH 8.4), and 1% deoxycholate (DOC) in the cathode chamber for 30 minutes at 40 mA. Protein samples in native 2$\times$ sample buffer (125 mM Tris [pH 6.8], 30% glycerol, and bromophenol blue) were size fractionated by electrophoresis for 40 minutes at 25 mA and transferred to a polyvinylidene difluoride (PVDF) membrane for Western blot analysis.

qRT PCR. Transfected HEK293T cells were directly lysed in TRIzol, and mRNA purification was performed according to the manufacturer's instructions. cDNA was generated from 1 μg of RNA with a first-strand cDNA synthesis kit. Real-time qPCR was performed with a StepOne instrument (Applied Biosystems) according to manufacturer's instruction. For the human GAPDH gene, forward primer 5′-GCAAATTCCATGGCACCGT and reverse primer 5′-TCGCCCCCACTTGATTTTGG were used. For the human 18S gene, the forward primer 5′-CTTCCACAGGAGGCCTACAC and reverse primer 5′-CGCAAAATATGCTGGAACTTT were used. For the human IFN-β gene, the forward primer 5′-ACGCCGCATTGACCATCTAT and reverse primer 5′-GTCTCATT CCAGCCAGTGCT were used. The IFN-β mRNA expression levels were normalized to the GAPDH mRNA expression. Changes in gene expression level were calculated by the threshold cycle ($2^{-\Delta\Delta CT}$) method. A two-tailed Student's *t* test was performed on ΔCT values to determine the *P* value (*, $P < 0.05$; **, $P < 0.01$; ***, $P < 0.001$).

Luciferase reporter assay. HEK293T cells were transfected with reporter plasmids (pIRF3-firefly luciferase and pIFN β-firefly luciferase), E6-encoding plasmids, and an internal control with pTK-*Renilla* luciferase. Cells were harvested 16 hours after transfection and assayed for luciferase activities with the Dual-Glo assay system (Promega, E2940). Results were expressed as a Firefly/*Renilla* luciferase ratio.

Peptide synthesis. Biotinylated peptides were synthesized by JPT Innovative Peptide Solutions with a purity higher than 70% (high-performance liquid chromatography [HPLC]). All peptides are N-terminally coupled to biotin via an *N*-(13-amino-4,7,10-trioxa-tridecayl)-succinamic acid (TTDS) linker. The lyophilized peptides were taken up into water to a stock concentration of 10 mM and stored at −20°C. The peptides were as follows: IRF3 peptide (EDILDELLGNMV), E6AP peptide (ELTLQELLGEER), Chim-E6AP-IRF3 (ELTLQELLGNMV), and Chim-IRF3-E6AP (EDILDELLGEER).

Protein expression and purification. The LxxLL construct consisted of a mutant bacterial maltose-binding protein (MBP*) followed by a triple alanine linker to the LxxLL peptide (MBP*-AAA-LxxLL). MBP* harbored six mutations (E360A, K363A, D364A, D83A, K84A, and K240A) to aid crystallization (54, 55). The IRF3-LxxLL sequence was EDILDELLGNMV. The E6 construct consisted of a His-tag followed by wild-type MBP and a TEV protease digestion site fused to the E6 protein (His$_6$-MBP-TEV-E6). The HPV16 E6 sequence harbored four stabilizing mutations of superficial cysteines (C80S, C97S, C111S, and C140S) to avoid oligomerization during purification and F47R mutation that prevents dimerization. Protein expression and purification were performed as described before (6, 7). Briefly, all MBP fusions were overexpressed separately in *Escherichia coli* BL21(DE3) cells in LB growth medium supplemented with 0.2% glucose and 50 μg/mL kanamycin. Expression was induced with 0.5 mM isopropyl-β-D-thiogalactopyranoside (IPTG), and 100 μM $ZnSO_4$ was added at the same time to ensure Zn2+ binding to E6. Induced cultures were incubated overnight at 16°C and 200 rpm. All constructs were purified separately by amylose affinity chromatography in buffer A (50 mM Tris [pH 6.8], 400 mM NaCl, and 2 mM dithiothreitol [DTT]) and eluted with 10 mM maltose in the same buffer. To remove soluble aggregates, all affinity-purified samples were ultracentrifuged at 110,000 $\times$ *g* in a swinging-bucket SW41 rotor (Beckman) for 16 h at 4°C. For crystallization, a His$_6$-MBP-E6 sample was digested with a TEV protease. The resulting E6 sample was concentrated and loaded separately onto a Superdex 75 or Superdex 200 (HiLoad 16/600) gel filtration column (GE Healthcare) equilibrated in buffer A for crystallization or buffer B for affinity assays (20 mM Tris [pH 7.5], 200 mM NaCl, and 2 mM DTT). All buffers were filtered, degassed, and saturated with argon before use.

Surface plasmon resonance (SPR) experiments. SPR binding experiments were performed on a Biacore T200 instrument (Cytiva, Biacore, Uppsala, Sweden) at 25°C as described previously (30). The running buffer was constituted by Tris buffer complemented with 0.005% (vol/vol) P20 surfactant (Cytiva). The four biotinylated synthetic peptides (IRF3, E6AP, chim-IRF3-E6AP, and chim-E6AP-IRF3) were reversibly captured on a sensor surface using the Biotin CAPture kit (Cytiva, Biacore product code 28-9202-34). Each cycle started by injecting CAPture reagent diluted five times in running buffer over all channels for 300 seconds at a 2-μL/minute flow rate. Capture levels were between 3,700 and 4,100 relative units (RU). Biotinylated peptides were immobilized by injecting a 40 nM solution at 20 μL/minute. Contact times were adjusted to reach peptide capture levels between 5 and 30 RU. In each cycle, a reference surface served as the control for nonspecific binding of the analyte and was treated as the peptide surfaces except that the peptide injection was omitted. The MBP-HPV16 E6 analyte was used at 720 nM and then injected on the four channels for 60 seconds at a flow rate of 30 μL/minute. The postinjection phase

was recorded for 180 additional seconds. At the end of each cycle, the surface was regenerated by injecting a 6 M guanidine hydrochloride solution supplemented with 250 mM sodium hydroxide for 60 seconds at 5 μL/minute followed by an additional washing step with the running buffer.

SPR data evaluation. The SPR signal recorded on the peptide surface was corrected systematically for the signals recorded from protein injection on the reference and from buffer injection on the peptide surface. Since peptides were captured at different levels, impeding a direct comparison of their corresponding SPR signals, corrected SPR responses were normalized according to $R_{norm} = R/R_{max}$, where R_{max}, the signal corresponding to the calculated maximal binding capacity of the surface, was obtained as follows: $R_{max} = R_{peptide} \times MW_{protein}/MW_{peptide}$. $R_{peptide}$ was the level of immobilized peptide (expressed in RU), while $MW_{peptide}$ and $MW_{protein}$ were the molecular masses of the peptide and protein, respectively.

Holdup experiment. Holdup is a comparative chromatographic retention assay (29, 31). The assay was performed in 96-well plates. A detailed manual holdup protocol as well as data acquisition and curation information have been described previously (30). Briefly, the analyte (MBP-HPV16 E6) was incubated either with ligand-saturated beads (here, biotinylated peptides) or with biotin-saturated beads to serve as a reference. After a 15-minute incubation of the analyte/beads mixture, a centrifugal filtration allowed the recovery of the liquid fraction containing the free analyte. The analyte concentration was quantified subsequently using a LabChip GX II (Caliper, PerkinElmer) device, which results in an electropherogram. The depletion of the analyte present in the liquid fraction, compared with the reference, is used to calculate a binding intensity (BI).

Crystallization. The HPV16 E6/IRF3-LxxLL complex was reconstituted by mixing MBP*-IRF3-LxxLL and HPV16 E6 (F47R, 4C/4S) samples in a 1:1 stoichiometric ratio in buffer C (50 mM Tris [pH 6.8], 200 mM NaCl, 2 mM DTT, and 5 mM maltose) and concentrated to 70 mg/mL before crystallization. Crystallization conditions were screened using kits available commercially (Qiagen, Hampton Research, Emerald Biosystems) by the sitting-drop vapor-diffusion method in 96-well MRC 2-drop plates (SWISSCI), employing a mosquito robot (TTP Labtech). Initial crystals were obtained and used as seeds during further optimization steps. After optimization, crystals grew in hanging drops containing 1.5 μL of protein solution at 70 mg/mL, 1.5 μL of reservoir solution containing 30% (vol/vol) polyethylene glycol (PEG) 1500, and 0.5 μL of seeds from the same conditions. Drops were equilibrated against 500 μL of reservoir solution at 293 K. Crystals were transferred sequentially through two cryosolutions of 20% (vol/vol) PEG 1500 + 5% (vol/vol) ethylene glycol and 32% (vol/vol) PEG 1500 + 5% (vol/vol) ethylene glycol. The crystals were flash cooled and stored in liquid nitrogen.

Data collection processing and structure determination. X-ray diffraction data were collected at the X06DA beamline at the Swiss Light Source (Villigen, Switzerland) synchrotron. Data were acquired from single cryocooled crystals (100 K) on a Pilatus-2M detector. The 360° data were collected using 0.2° rotation and 0.2-second exposure time with 20% beam attenuation for each image. Data sets were indexed, processed, and scaled using XDS. Data collection and refinement statistics are summarized in Table 1. E6/IRF3-LxxLL crystal diffracted up to a resolution of 1.50 Å, belonged to the orthorombic space group $P2_12_12$ with unit cell parameters a = 97.66 Å, b = 132.87 Å, and c = 43.03 Å and a refined crystal mosaicity of 0.26 Å. The asymmetric unit contained one copy of the E6/MBP-IRF3-LxxLL heterodimer, with a corresponding Matthew's coefficient of 2.32 $Å^3$ per Dalton and a solvent content of 47%. Resolution was set to that at which $CC_{1/2}$ was higher than 0.5 (56, 57) and was confirmed running PDB_REDO (58). The structure was solved by two sequential molecular replacements using Phaser and the structures of MBP and E6/E6AP-LxxLL complex from PDB 4GIZ as search models. Crystallographic refinement involved repeated cycles of conjugate-gradient energy minimization and temperature-factor refinement and was performed using PHENIX followed by iterative model building in Coot. B-factors were refined as anisotropic for all atoms except for hydrogens and water molecules. HPV16-E6 residues 1 to 6 and 141 to 151 did not present enough electron density to be built and were not included in the PDB file. The quality of the refined models was assessed using MOLPROBITY. All molecular graphics figures were produced using PyMOL (The PyMOL Molecular Graphics System, version 1.7; Schrödinger, LLC). E6 residues at interface regions were identified by the observation of an increase in solvent accessible surface area (SASA) obtained upon removal of the corresponding LxxLL peptide from the PDB file of the complex. Positive changes in SASA values indicate E6 residues in atomic contact with the IRF3 peptide. The refined model and the structure factor amplitude have been deposited in the PDB and are available under accession number 6SJA.

Free-energy decomposition analysis. Estimates of the individual amino acid contributions to the binding free energy related to complex formation were obtained from the crystallographic structures representing the conformational space sampled during the molecular dynamics (MD) simulations. The free-energy analysis was performed using the Molecular Mechanics Poisson Bolzmann Surface Area (MM/PBSA) free-energy decomposition scheme presented as described previously (59).

Data availability. Data have been deposited in PDB entries 6SJA and 4GIZ.

ACKNOWLEDGMENTS

This work was supported by the CNRS, the University of Strasbourg, the ANR, the Infect-Era 2015 ("HPV motiva" project), the Ligue Contre le Cancer (CCIR-GE and "équipe labelisée" 2015 to G.T.), the National Institutes of Health (grant R01CA134737 to G.T.), the Canceropôle Grand Est, Alsace Contre le Cancer, and a grant of Fondation pour la Recherche Médicale (FRM) to I.P.S.

We thank Denise Galloway for the generous gift of keratinocyte cell lines (HFK-LXSN and HFK-LXSN-16E6). We thank Françoise Bachelerie for helpful discussion and Marc Vigneron for critical reading of the manuscript. We acknowledge the support and the use of resources of the French Infrastructure for Integrated Structural Biology FRISBI ANR-10-INBS-05 and of Instruct-ERIC, the Swiss Light Source synchrotron (P. Scherrer Institute, Villigen, Switzerland), and the beam scientists at the PXIII beamline.

Conceived and designed the experiments. G.T. and M.M.; performed experiments, J.P., I.P.S., A.C.-S., M.-L.S., P.P., E.H., A.F., A.M., N.M., S.R., and M.M.; contributed reagents/material/analysis tools, D.G. and C.G.; analyzed the data, I.P.S., Y.C., D.A., A.P., G.T., and Y.N.; wrote the paper, M.M.

REFERENCES

1. Dufour X, Beby-Defaux A, Agius G, Lacau St Guily J. 2012. HPV and head and neck cancer. Eur Ann Otorhinolaryngol Head Neck Dis 129:26–31. https://doi.org/10.1016/j.anorl.2011.05.004.
2. Orth G. 2006. Genetics of epidermodysplasia verruciformis: insights into host defense against papillomaviruses. Semin Immunol 18:362–374. https://doi.org/10.1016/j.smim.2006.07.008.
3. Jablonska S, Dabrowski J, Jakubowicz K. 1972. Epidermodysplasia verruciformis as a model in studies on the role of papovaviruses in oncogenesis. Cancer Res 32:583–589.
4. Rollison DE, Viarisio D, Amorrortu RP, Gheit T, Tommasino M. 2019. An emerging issue in oncogenic virology: the role of beta human papillomavirus types in the development of cutaneous squamous cell carcinoma. J Virol 93:D499. https://doi.org/10.1128/JVI.01003-18.
5. McLaughlin-Drubin ME, Munger K. 2009. Oncogenic activities of human papillomaviruses. Virus Res 143:195–208. https://doi.org/10.1016/j.virusres.2009.06.008.
6. Zanier K, Charbonnier S, Sidi AOMO, McEwen AG, Ferrario MG, Poussin-Courmontagne P, Cura V, Brimer N, Babah KO, Ansari T, Muller I, Stote RH, Cavarelli J, Vande Pol S, Travé G. 2013. Structural basis for hijacking of cellular LxxLL motifs by papillomavirus E6 oncoproteins. Science 339:694–698. https://doi.org/10.1126/science.1229934.
7. Martinez-Zapien D, Ruiz FX, Poirson J, Mitschler A, Ramirez J, Forster A, Cousido-Siah A, Masson M, Vande Pol S, Podjarny A, Travé G, Zanier K. 2016. Structure of the E6/E6AP/p53 complex required for HPV-mediated degradation of p53. Nature 529:541–545. https://doi.org/10.1038/nature16481.
8. Wu J, Chen ZJ. 2014. Innate immune sensing and signaling of cytosolic nucleic acids. Annu Rev Immunol 32:461–488. https://doi.org/10.1146/annurev-immunol-032713-120156.
9. Liu S, Cai X, Wu J, Cong Q, Chen X, Li T, Du F, Ren J, Wu Y-T, Grishin NV, Chen ZJ. 2015. Phosphorylation of innate immune adaptor proteins MAVS, STING, and TRIF induces IRF3 activation. Science 347:aaa2630. https://doi.org/10.1126/science.aaa2630.
10. Fitzgerald KA, McWhirter SM, Faia KL, Rowe DC, Latz E, Golenbock DT, Coyle AJ, Liao S-M, Maniatis T. 2003. IKKepsilon and TBK1 are essential components of the IRF3 signaling pathway. Nat Immunol 4:491–496. https://doi.org/10.1038/ni921.
11. Perry AK, Chow EK, Goodnough JB, Yeh W-C, Cheng G. 2004. Differential requirement for TANK-binding kinase-1 in type I interferon responses to toll-like receptor activation and viral infection. J Exp Med 199:1651–1658. https://doi.org/10.1084/jem.20040528.
12. Panne D, Maniatis T, Harrison SC. 2007. An atomic model of the interferon-beta enhanceosome. Cell 129:1111–1123. https://doi.org/10.1016/j.cell.2007.05.019.
13. Ford E, Thanos D. 2010. The transcriptional code of human IFN-beta gene expression. Biochim Biophys Acta 1799:328–336. https://doi.org/10.1016/j.bbagrm.2010.01.010.
14. Borden EC. 2019. Interferons α and β in cancer: therapeutic opportunities from new insights. Nat Rev Drug Discov 18:219–234. https://doi.org/10.1038/s41573-018-0011-2.
15. Sunthamala N, Thierry F, Teissier S, Pientong C, Kongyingyoes B, Tangsiriwatthana T, Sangkomkamhang U, Ekalaksananan T. 2014. E2 proteins of high risk human papillomaviruses down-modulate STING and IFN-κ transcription in keratinocytes. PLoS One 9:e91473. https://doi.org/10.1371/journal.pone.0091473.
16. Hasan UA, Bates E, Takeshita F, Biliato A, Accardi R, Bouvard V, Mansour M, Vincent I, Gissmann L, Iftner T, Sideri M, Stubenrauch F, Tommasino M. 2007. TLR9 expression and function is abolished by the cervical cancer-associated human papillomavirus type 16. J Immunol 178:3186–3197. https://doi.org/10.4049/jimmunol.178.5.3186.
17. Lau L, Gray EE, Brunette RL, Stetson DB. 2015. DNA tumor virus oncogenes antagonize the cGAS-STING DNA-sensing pathway. Science 350:568–571. https://doi.org/10.1126/science.aab3291.
18. Luo X, Donnelly CR, Gong W, Heath BR, Hao Y, Donnelly LA, Moghbeli T, Tan YS, Lin X, Bellile E, Kansy BA, Carey TE, Brenner JC, Cheng L, Polverini PJ, Morgan MA, Wen H, Prince ME, Ferris RL, Xie Y, Young S, Wolf GT, Chen Q, Lei YL. 2020. HPV16 drives cancer immune escape via NLRX1-mediated degradation of STING. J Clin Invest 130:1635–1652. https://doi.org/10.1172/JCI129497.
19. Cigno Lo I, Calati F, Borgogna C, Zevini A, Albertini S, Martuscelli L, De Andrea M, Hiscott J, Landolfo S, Gariglio M. 2020. Human papillomavirus E7 oncoprotein subverts host innate immunity via SUV39H1-mediated epigenetic silencing of immune sensor genes. J Virol 94:e01812-19. https://doi.org/10.1128/JVI.01812-19.
20. Chiang C, Pauli E-K, Biryukov J, Feister KF, Meng M, White EA, Munger K, Howley PM, Meyers C, Gack MU. 2018. The human papillomavirus E6 oncoprotein targets USP15 and TRIM25 to suppress RIG-I-mediated innate immune signaling. J Virol 92:e01737-17. https://doi.org/10.1128/JVI.01737-17.
21. Ronco LV, Karpova AY, Vidal M, Howley PM. 1998. Human papillomavirus 16 E6 oncoprotein binds to interferon regulatory factor-3 and inhibits its transcriptional activity. Genes Dev 12:2061–2072. https://doi.org/10.1101/gad.12.13.2061.
22. Li S, Labrecque S, Gauzzi MC, Cuddihy AR, Wong AH, Pellegrini S, Matlashewski GJ, Koromilas AE. 1999. The human papilloma virus (HPV)-18 E6 oncoprotein physically associates with Tyk2 and impairs Jak-STAT activation by interferon-alpha. Oncogene 18:5727–5737. https://doi.org/10.1038/sj.onc.1202960.
23. Strähle L, Garcin D, Kolakofsky D. 2006. Sendai virus defective-interfering genomes and the activation of interferon-beta. Virology 351:101–111. https://doi.org/10.1016/j.virol.2006.03.022.
24. Brant AC, Menezes AN, Felix SP, de Almeida LM, Sammeth M, Moreira MAM. 2019. Characterization of HPV integration, viral gene expression and E6E7 alternative transcripts by RNA-Seq: a descriptive study in invasive cervical cancer. Genomics 111:1853–1861. https://doi.org/10.1016/j.ygeno.2018.12.008.
25. Suarez I, Travé G. 2018. Structural insights in multifunctional papillomavirus oncoproteins. Viruses 10:37. https://doi.org/10.3390/v10010037.
26. Shah M, Anwar MA, Park S, Jafri SS, Choi S. 2015. In silico mechanistic analysis of IRF3 inactivation and high-risk HPV E6 species-dependent drug response. Sci Rep 5:13446. https://doi.org/10.1038/srep13446.
27. Cassonnet P, Rolloy C, Neveu G, Vidalain P-O, Chantier T, Pellet J, Jones L, Muller M, Demeret C, Gaud G, Vuillier F, Lotteau V, Tangy F, Favre M, Jacob Y. 2011. Benchmarking a luciferase complementation assay for detecting protein complexes. Nat Methods 8:990–992. https://doi.org/10.1038/nmeth.1773.
28. Poirson J, Biquand E, Straub M-L, Cassonnet P, Nominé Y, Jones L, van der Werf S, Travé G, Zanier K, Jacob Y, Demeret C, Masson M. 2017. Mapping the interactome of HPV E6 and E7 oncoproteins with the ubiquitin-proteasome system. FEBS J 284:3171–3201. https://doi.org/10.1111/febs.14193.
29. Vincentelli R, Luck K, Poirson J, Polanowska J, Abdat J, Blémont M, Turchetto J, Iv F, Ricquier K, Straub M-L, Forster A, Cassonnet P, Borg J-P, Jacob Y, Masson M, Nominé Y, Reboul J, Wolff N, Charbonnier S, Travé G.

2015. Quantifying domain-ligand affinities and specificities by high-throughput holdup assay. Nat Methods 12:787–793. https://doi.org/10.1038/nmeth.3438.
30. Bonhoure A, Forster A, Babah KO, Gógl G, Eberling P, Kostmann C, Volkmer R, Tapia Mancilla V, Travé G, Nominé Y. 2020. Benchtop holdup assay for quantitative affinity-based analysis of sequence determinants of protein-motif interactions. Anal Biochem 603:113772. https://doi.org/10.1016/j.ab.2020.113772.
31. Jané P, Chiron L, Bich G, Travé G, Nominé Y. 2021. A computational protocol to analyze PDZ/PBM affinity data obtained by high-throughput holdup assay. Methods Mol Biol 2256:61–74. https://doi.org/10.1007/978-1-0716-1166-1_4.
32. Panne D, McWhirter SM, Maniatis T, Harrison SC. 2007. Interferon regulatory factor 3 is regulated by a dual phosphorylation-dependent switch. J Biol Chem 282:22816–22822. https://doi.org/10.1074/jbc.M703019200.
33. Yoneyama M, Suhara W, Fukuhara Y, Fukuda M, Nishida E, Fujita T. 1998. Direct triggering of the type I interferon system by virus infection: activation of a transcription factor complex containing IRF-3 and CBP/p300. EMBO J 17:1087–1095. https://doi.org/10.1093/emboj/17.4.1087.
34. Ortega E, Rengachari S, Ibrahim Z, Hoghoughi N, Gaucher J, Holehouse AS, Khochbin S, Panne D. 2018. Transcription factor dimerization activates the p300 acetyltransferase. Nature 562:538–544. https://doi.org/10.1038/s41586-018-0621-1.
35. Yang H, Lin CH, Ma G, Orr M, Baffi MO, Wathelet MG. 2002. Transcriptional activity of interferon regulatory factor (IRF)-3 depends on multiple protein-protein interactions. Eur J Biochem 269:6142–6151. https://doi.org/10.1046/j.1432-1033.2002.03330.x.
36. Lin CH, Hare BJ, Wagner G, Harrison SC, Maniatis T, Fraenkel E. 2001. A small domain of CBP/p300 binds diverse proteins: solution structure and functional studies. Mol Cell 8:581–590. https://doi.org/10.1016/s1097-2765(01)00333-1.
37. Qin BY, Liu C, Srinath H, Lam SS, Correia JJ, Derynck R, Lin K. 2005. Crystal structure of IRF-3 in complex with CBP. Structure 13:1269–1277. https://doi.org/10.1016/j.str.2005.06.011.
38. Patel D, Huang SM, Baglia LA, McCance DJ. 1999. The E6 protein of human papillomavirus type 16 binds to and inhibits co-activation by CBP and p300. EMBO J 18:5061–5072. https://doi.org/10.1093/emboj/18.18.5061.
39. Howie HL, Koop JI, Weese J, Robinson K, Wipf G, Kim L, Galloway DA. 2011. Beta-HPV 5 and 8 E6 promote p300 degradation by blocking AKT/p300 association. PLoS Pathog 7:e1002211. https://doi.org/10.1371/journal.ppat.1002211.
40. Schwanke H, Stempel M, Brinkmann MM. 2020. Of keeping and tipping the balance: host regulation and viral modulation of IRF3-dependent IFNB1 expression. Viruses 12:733. https://doi.org/10.3390/v12070733.
41. Gheit T. 2019. Mucosal and cutaneous human papillomavirus infections and cancer biology. Front Oncol 9:355. https://doi.org/10.3389/fonc.2019.00355.
42. Bouvard V, Baan R, Straif K, Grosse Y, Secretan B, Ghissassi EF, Benbrahim-Tallaa L, Guha N, Freeman C, Galichet L, Cogliano V, WHO International Agency for Research on Cancer Monograph Working Group. 2009. A review of human carcinogens–part B: biological agents. Lancet Oncol 10:321–322. https://doi.org/10.1016/s1470-2045(09)70096-8.
43. Zimmermann H, Degenkolbe R, Bernard HU, O'Connor MJ. 1999. The human papillomavirus type 16 E6 oncoprotein can down-regulate p53 activity by targeting the transcriptional coactivator CBP/p300. J Virol 73:6209–6219. https://doi.org/10.1128/JVI.73.8.6209-6219.1999.
44. Thomas MC, Chiang C-M. 2005. E6 oncoprotein represses p53-dependent gene activation via inhibition of protein acetylation independently of inducing p53 degradation. Mol Cell 17:251–264. https://doi.org/10.1016/j.molcel.2004.12.016.
45. Xie X, Piao L, Bullock BN, Smith A, Su T, Zhang M, Teknos TN, Arora PS, Pan Q. 2014. Targeting HPV16 E6-p300 interaction reactivates p53 and inhibits the tumorigenicity of HPV-positive head and neck squamous cell carcinoma. Oncogene 33:1037–1046. https://doi.org/10.1038/onc.2013.25.
46. Lin R, Mamane Y, Hiscott J. 1999. Structural and functional analysis of interferon regulatory factor 3: localization of the transactivation and autoinhibitory domains. Mol Cell Biol 19:2465–2474. https://doi.org/10.1128/MCB.19.4.2465.
47. Qin BY, Liu C, Lam SS, Srinath H, Delston R, Correia JJ, Derynck R, Lin K. 2003. Crystal structure of IRF-3 reveals mechanism of autoinhibition and virus-induced phosphoactivation. Nat Struct Biol 10:913–921. https://doi.org/10.1038/nsb1002.
48. Kumar KP, McBride KM, Weaver BK, Dingwall C, Reich NC. 2000. Regulated nuclear-cytoplasmic localization of interferon regulatory factor 3, a subunit of double-stranded RNA-activated factor 1. Mol Cell Biol 20:4159–4168. https://doi.org/10.1128/MCB.20.11.4159-4168.2000.
49. Chattopadhyay S, Marques JT, Yamashita M, Peters KL, Smith K, Desai A, Williams BRG, Sen GC. 2010. Viral apoptosis is induced by IRF-3-mediated activation of Bax. EMBO J 29:1762–1773. https://doi.org/10.1038/emboj.2010.50.
50. Duguay D, Mercier F, Stagg J, Martineau D, Bramson J, Servant M, Lin R, Galipeau J, Hiscott J. 2002. In vivo interferon regulatory factor 3 tumor suppressor activity in B16 melanoma tumors. Cancer Res 62:5148–5152.
51. Kim TY, Lee K-H, Chang S, Chung C, Lee H-W, Yim J, Kim TK. 2003. Oncogenic potential of a dominant negative mutant of interferon regulatory factor 3. J Biol Chem 278:15272–15278. https://doi.org/10.1074/jbc.M205792200.
52. Wallace NA, Khanal S, Robinson KL, Wendel SO, Messer JJ, Galloway DA. 2017. High-risk alphapapillomavirus oncogenes impair the homologous recombination pathway. J Virol 91:e01084-17. https://doi.org/10.1128/JVI.01084-17.
53. Strähle L, Marq J-B, Brini A, Hausmann S, Kolakofsky D, Garcin D. 2007. Activation of the beta interferon promoter by unnatural Sendai virus infection requires RIG-I and is inhibited by viral C proteins. J Virol 81:12227–12237. https://doi.org/10.1128/JVI.01300-07.
54. Kobe B, Center RJ, Kemp BE, Poumbourios P. 1999. Crystal structure of human T cell leukemia virus type 1 gp21 ectodomain crystallized as a maltose-binding protein chimera reveals structural evolution of retroviral transmembrane proteins. Proc Natl Acad Sci U S A 96:4319–4324. https://doi.org/10.1073/pnas.96.8.4319.
55. Moon AF, Mueller GA, Zhong X, Pedersen LC. 2010. A synergistic approach to protein crystallization: combination of a fixed-arm carrier with surface entropy reduction. Protein Sci 19:901–913. https://doi.org/10.1002/pro.368.
56. Karplus PA, Diederichs K. 2012. Linking crystallographic model and data quality. Science 336:1030–1033. https://doi.org/10.1126/science.1218231.
57. Karplus PA, Diederichs K. 2015. Assessing and maximizing data quality in macromolecular crystallography. Curr Opin Struct Biol 34:60–68. https://doi.org/10.1016/j.sbi.2015.07.003.
58. Joosten RP, Long F, Murshudov GN, Perrakis A. 2014. The PDB_REDO server for macromolecular structure model optimization. IUCrJ 1:213–220. https://doi.org/10.1107/S2052252514009324.
59. Lafont V, Schaefer M, Stote RH, Altschuh D, Dejaegere A. 2007. Protein-protein recognition and interaction hot spots in an antigen-antibody complex: free energy decomposition identifies "efficient amino acids." Proteins 67:418–434. https://doi.org/10.1002/prot.21259.